Journal of Applied Physics

Initial transient stage of pin-to-pin nanosecond repetitively pulsed discharges in air

Cite as: J. Appl. Phys. **132**, 013301 (2022); https://doi.org/10.1063/5.0093794
Submitted: 30 March 2022 • Accepted: 19 June 2022 • Published Online: 05 July 2022

Xingxing Wang, Adam Patel and Alexey Shashurin

Journal of Applied Physics ARTICLE scitation.org/journal/jap

Initial transient stage of pin-to-pin nanosecond repetitively pulsed discharges in air

Cite as: J. Appl. Phys. **132**, 013301 (2022); doi: 10.1063/5.0093794
Submitted: 30 March 2022 · Accepted: 19 June 2022 ·
Published Online: 5 July 2022

Xingxing Wang, Adam Patel, and Alexey Shashurin[a)]

AFFILIATIONS

School of Aeronautics and Astronautics, Purdue University, 701 W Stadium Ave., West Lafayette, Indiana 47907, USA

[a)]**Author to whom correspondence should be addressed:** ashashur@purdue.edu

ABSTRACT

In this work, evolution of parameters of nanosecond repetitively pulsed (NRP) discharges in pin-to-pin configuration in air was studied during the transient stage of initial 20 discharge pulses. Gas and plasma parameters in the discharge gap were measured using coherent microwave scattering, optical emission spectroscopy, and laser Rayleigh scattering for NRP discharges at repetition frequencies of 1, 10, and 100 kHz. Memory effects (when perturbations induced by the previous discharge pulse would not decay fully until the subsequent pulse) were detected for the repetition frequencies of 10 and 100 kHz. For 10 kHz NRP discharge, the discharge parameters experienced significant change after the first pulse and continued to substantially fluctuate between subsequent pulses due to rapid evolution of gas density and temperature during the 100 μs inter-pulse time caused by intense redistribution of the flow field in the gap on that time scale. For 100 kHz NRP discharge, the discharge pulse parameters reached a new steady-state at about five pulses after initiation. This new steady-state was associated with well-reproducible parameters between the discharge pulses and substantial reduction in breakdown voltage, discharge pulse energy, and electron number density in comparison to the first discharge pulse. For repetition frequencies 1–100 kHz considered in this work, the memory effects can be likely attributed to the reduction in gas number density and increase in the gas temperature that cannot fully recover to ambient conditions before subsequent discharge pulses.

I. INTRODUCTION

Nanosecond discharges (ns-discharges) have drawn great interest due to a wide variety of potential applications. The ns-scale rise time of high voltage driving pulse allows the voltage to quickly increase beyond the breakdown voltage threshold that enables efficient energy deposition into an interelectrode gas volume and production of active species.[1] Utilization of series of ns-discharges applied at repetition frequencies in the kHz range refers to a nanosecond repetitively pulsed (NRP) discharge. The NRP discharges found applications in plasma-assisted combustion owing to generation of gaseous species including O, H, OH, etc.[2–4] Additionally, NRP discharges can be used for aerodynamic flow control applications (plasma actuators) that utilize NRP-driven energy deposition into gas in vicinity of airfoil surface to delay flow separation and reduce drag.[5,6] NRP discharges have been also utilized in many other fields including medicine, nanotechnology, material processing, sterilization, etc.[7]

In our previous work,[8] ns-discharge in air in pin-to-pin configuration with 5 mm gap operating in the single-pulse mode was studied. Two discharge regimes were observed (spark and corona) and characterized. In the spark regime, about 5 mJ nanosecond discharge pulse produced plasmas with electron number density of approximately 5×10^{15} cm^{-3} and characteristic decay time of 150–200 ns. The gas temperature increase to 3500 K at 10 μs after the discharge was measured by optical emission spectroscopy (OES), and the gas density decrease to a minimum of 30% of ambient value 5 μs after the discharge was detected by laser Rayleigh scattering. Similar trends of gas density and temperature were also observed in numerical simulations by Popov.[9] Both gas temperature and gas number density recover to ambient conditions within about 1 ms after the discharge pulse. Therefore, one should expect the onset of memory effects (when perturbations induced by the previous discharge pulse would not decay fully until the subsequent pulse) at repetition frequency higher than 1 kHz. In general, the memory effects in ns-discharges reported in literature were attributed to accumulation of residual species remaining post-discharge in the interelectrode gas volume and on the adjacent surfaces (electrons and ions, excited and atomic particles).[10–12]

NRP pin-to-pin discharges operating at repetition frequencies in kHz range have been studied by many other groups. In the works by Pai *et al.* and Rusterholtz *et al.*,[13–15] NRP pin-to-pin discharges at 10–30 kHz were studied in a preheated air at 1000 K where the gap distance between electrodes was kept at 4–5 mm. With an energy input of <1 mJ, gas temperature was measured to be up to 5000 K, and the electron number density was on the order of 10^{15} cm^{-3}. In the work by Horst *et al.*,[16] NRP pin-to-pin discharge was studied in N_2 and 0.9% humidified N_2. The discharges were operating at a repetition frequency of 1 kHz at atmospheric conditions with a gap of 2 mm. The gas temperature was measured to be up to 750 K at the moment 1 μs after the nanosecond pulse, and the electron number density was reported to be on the order of 10^{16} cm^{-3} when the energy input per pulse is around 1 mJ.

Therefore, air-based NRP discharges in pin-to-pin configuration operating in the kHz frequency range were studied previously. However, parameters of these discharges were mostly studied on a later stage well after initiation of sequence of discharge pulses while transition of parameters from pulse No. 1 to the later pulses was not thoroughly studied. In this work, transient dynamics of gas and plasma parameters for first 20 pulses after NRP discharge initiation for different discharge repetition frequencies was studied.

II. EXPERIMENTAL SETUP AND METHODOLOGY

The experimental setup utilized HV nanosecond pulse supplied by an ns-pulser (Eagle Harbor NSP-3300-20-F) to initiate NRP discharges and pin-to-pin discharge electrodes separated 5 mm apart. The pulser is optimized to operate with 800 Ω resistive load and produce rectangular pulses with peak voltage up to 25 kV, pulse duration of 30–110 ns (90 ns pulse width was used in this work), and repetition frequency up to 400 kHz. In this work, a standard Eagle Harbor matching resistor stage (comprised of a 5 kΩ resistor connected in parallel and two 260 Ω resistors connected in series with the discharge assembly) was used to improve the impedance matching. More details on the utilized circuitry, pulser characteristics, and equivalent impedance of the discharge plasma channel on the different stages of the discharge event can be found in Ref. 8. Voltage (V) and current (I) measurements were conducted by conventional voltage probes (Tektronix P6015A) and a current transformer (Bergoz FCT-028-0.5-WB). Gas temperature T_{gas} (=rotational temperature T_{rot})[17] was measured by optical emission spectroscopy (OES) of a nitrogen second positive system (SPS) using a Princeton Instruments SP-2750i spectrometer and a Princeton Instruments PI-MAX 1024i ICCD camera. This OES system was previously developed and utilized for gas temperature measurements during and after single-pulse ns-discharges with 5 ns temporal resolution and 200 μm spatial resolution (measurements after the discharge when the gas is not glowing were conducted by using probing ns-pulse to excite SPS of N_2 while ensuring that heating by the probing pulse itself is negligible).[8,17] In this work, the pre-pulse gas temperature T_{g0} was determined using the same method; namely, by conducting the OES measurements during first 5 ns of the discharge pulse when SPS of N_2 is detectable while heating of the gas is still negligible.[8,17] Gas density (n_g) measurements were conducted by laser Rayleigh scattering (LRS) using a nanosecond laser at 532 nm supplied by EKSPLA NT342 (temporal resolution—5 ns, spatial resolution—320 μm). Finally, electron number density (n_e) was measured using coherent microwave scattering (CMS) combined with LRS (temporal resolution < 1 ns). The experimental setup and diagnostic techniques were identical to one used in our previous work.[8]

Gas temperature T_{gas} and bulk gas density n_g were recorded at pulse Nos. 1, 2, 3, 4, 5, 10, and 20 of the burst. T_{gas} on each pulse was recorded at the beginning of the ns-pulse representing the initial condition of temperature for the corresponding discharge. The timing of the ICCD camera gate was controlled via the gate delay setting in Lightfield software. Two measurements of n_g were recorded for each discharge pulse by sending the laser pulses at desired moments controlled by an external waveform generator. Specifically, the laser pulses were sent right before the initiation of the discharge pulse for the measurement of initial condition of n_g of each discharge (n_{g0}) and 5 μs after the initiation of the discharge pulse that is expected to be representative for the lowest gas number density after discharge ($n_{g,min}$) (based on previous measurements indicating that the gas density in the gap dropped about a 1 μs post-discharge, remained nearly constant for tens of μs, and then recovered to the ambient level in the next 1 ms).[8,18] In order to reach an adequate signal-to-noise ratio, 100 accumulations were taken for the OES measurement and 10 accumulations were used for the LRS measurement.

For the CMS system, n_e was determined from the output CMS signal U_s using following expression:[19] $U_s = \frac{Ae^2 n_e V}{m\sqrt{\omega^2+\nu_m^2}}$, where A is the CMS system calibration factor (determined using calibration with dielectric scatterers), V is the plasma volume (determined using ICCD photography), ν_m is the electron-gas collisional frequency (determined based on LRS measurements), ω is the microwave frequency, and m and e are electron mass and charge. More details on n_e-measurements by means of combination of CMS and LRS techniques can be found elsewhere.[8,19]

III. RESULTS AND DISCUSSION

The temporal evolution of discharge parameters for a burst of 20 pulses applied at repetition rate of $f = 1$ kHz is presented in Fig. 1 including discharge voltage (V_d), discharge current (I_d), pulse energy (E_{pulse}, calculated by integrating the product of voltage and current over pulse duration), and pre-pulse gas temperature (T_{g0}) and density (n_{g0}) measured right before the initiation of corresponding discharge pulse. Note that Figs. 1(a) and 1(b) intentionally present temporally unresolved dynamics for V_d and I_d to trace evolution of peak values of corresponding properties in the burst, namely, breakdown voltage V_{br} and peak discharge current I_{peak}. Additionally, n_e plotted in Fig. 1(f) was determined from Eq. (1) using measured microwave scattering signal U_s, plasma volume of V = 2.5×10^{-4} cm^3 (a cylinder with height of 5 mm and diameter of 250 μm) determined using ICCD camera, and following approximation for collisional frequency $\nu_m = \frac{1.42\times10^{12}}{2.5\times10^{19}} n_{g0}(\text{cm}^{-3})$, s^{-1} used in combination with measured n_{g0} dynamics across pulses in the burst.[19] The utilized approximations for V and ν_m are valid during the ns-discharge pulse while deviate on the decay stage;[8,18] therefore, Fig. 1(f) allows to trace evolution of peak electron

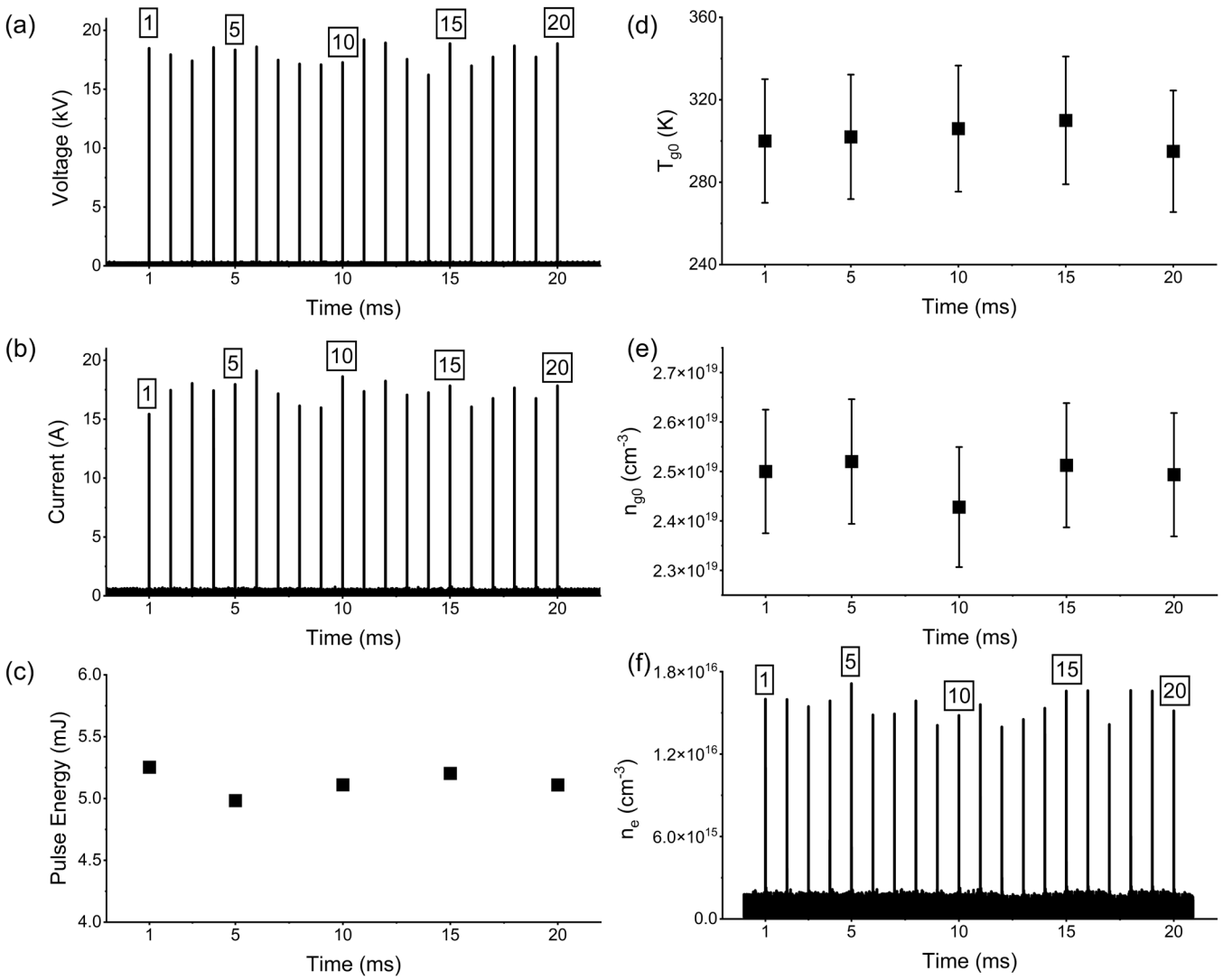

FIG. 1. Temporal evolution of parameters for NRP discharge at $f = 1$ kHz. (a) Voltage (V_d); (b) current (I_d); (c) discharge pulse energy (E_{pulse}); (d) gas temperature T_{g0} right before discharge pulse initiation (for pulse Nos. 1, 5, 10, 15, and 20); (e) gas number density n_{g0} right before discharge pulse initiation (for pulses Nos. 1, 5, 10, 15, and 20); and (f) electron number density n_e.

number density $n_{e,peak}$ along the pulses in the burst while details of electron decay are intentionally unresolved in time.

One can see in Fig. 1 that discharge parameters were similar between different pulses in the burst and experienced fairly small variations (on the order of ±6%, ±12%, ±2%, ±6%, ±3%, and ±10% for V_{br}, I_{peak}, E_{pulse}, T_{g0}, n_{g0}, and $n_{e,peak}$, respectively) around corresponding steady-state values ($V_{br} = 19$ kV, $I_{peak} = 16$ A, $E_{pulse} = 5.1$ mJ, $T_{g0} = 300$ K, $n_{g0} = 2.5 \times 10^{19}$ cm^{-3}, and $n_{e,peak} = 1.5 \times 10^{16}$ cm^{-3}). These variations between the discharge pulses are associated with natural irreproducibility of the streamer breakdown and microscale changes of the cathode morphology due to cathode spot presence on the later stage of the discharge pulse.[8] Temporally resolved discharge voltage and current waveforms were also consistent across the pulses in the burst, and typical evolutions of V_d and I_d are shown in Fig. 2 (for pulse No. 10). Thus, it might be concluded that each discharge pulse in the burst closely resembles pulse No. 1, which indicates that no memory effects between the pulses are present. [Note that the current waveform shown in Fig. 2 displays the total current comprised of displacement and conductivity currents. The displacement current was dominant before the breakdown ($t < 30$ ns), while the conductivity current was governing after the breakdown ($t > 30$ ns).] This conclusion is consistent with our recent findings that gas parameters (n_g and T_g) in the

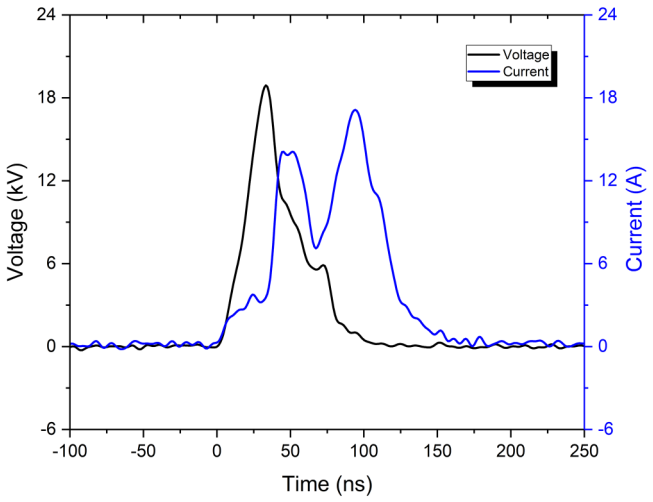

FIG. 2. Typical temporal evolution of discharge voltage (black) and discharge current (blue) for pulses in the burst (f = 1 kHz, pulse No. 10).

gap fully recover to their initial unperturbed pre-discharge values on times ~1 ms after the ns-pulse.[8] Therefore, each subsequent discharge pulse in the burst occurs in the gas of essentially same properties (300 K, 2.5×10^{19} cm^{-3}) yielding similar discharge parameters for all pulses.

Evolution of discharge parameters for a burst of 20 pulses at the repetition rate of $f = 10$ kHz is presented in Fig. 3 (note that n_e was determined using same approximations for $V = 2.5\times10^{-4}$ cm^3 and $\nu_m = \frac{1.42\times10^{12}}{2.5\times10^{19}} n_{g0}(\text{cm}^{-3})$, s^{-1} as above for $f = 1$ kHz). One can see that discharge parameters of the first pulse substantially differ from that of consecutive pulses. Specifically, V_{br}, E_{pulse}, and $n_{e,peak}$ decreased from 18 kV, 5.2 mJ, and 1.5×10^{16} cm^{-3} for pulse No. 1 to 5–14.5 kV, 2.6–3.8 mJ, and $2.5–5\times10^{15}$ cm^{-3} for pulse Nos. 2–20. This change of parameters can be explained by a memory effect; namely, gas number density and temperature do not recover to their initial unperturbed values of 300 K and 2.5×10^{19} cm^{-3} by the time of the second pulse arrival. Indeed, Fig. 3(c) supports that gas temperature and number density before the second pulse were substantially different, namely, $T_{g0} = 1600$ K and $n_{g0} = 1.1\times10^{19}$ cm^{-3}. Finally, the memory effects were preserved for the entire duration of the burst given that T_g and n_g never recover to their initial unperturbed values (300 K, 2.5×10^{19} cm^{-3}) as one can see in Figs. 3(d) and 3(e).

Starting from pulse No. 2, the discharge pulse parameters shown in Fig. 3 settle on a new steady-state values of $V_{br} = 9.5$ kV, $I_{peak} = 20$ A, $E_{pulse} = 3.2$ mJ, $T_{g0} = 1100$ K, $n_{g0} = 1.0\times10^{19}$ cm^{-3}, and $n_{e,peak} = 3.7\times10^{15}$ cm^{-3}, which are different from that at $f = 1$ kHz. Additionally, these new steady-state values are associated with more substantial variability between the pulses compared to the case of $f = 1$ kHz; namely, variations of V_{br}, I_{peak}, E_{pulse}, T_{g0}, n_{g0}, and $n_{e,peak}$ were ±49%, ±13%, ±14%, ±10%, ±13%, and ±35%, respectively. This larger variability of discharge pulse parameters refers to the fact that moment of subsequent pulse initiation coincides with the region of rapid temporal change of T_g and n_g, which is associated with intense redistribution of the flow field in the gap on a 100 μs inter-pulse time scale.[20] Indeed, our recent measurements confirm a very rapid change of T_g and n_g during 100 μs after the first discharge pulse (about 60% drop for T_g and 30% increase for and n_g, respectively).[8] Additionally, minimal number density for each discharge pulse, $n_{g,min}$, (which establishes on a μs-timescale after the discharge pulse)[8] is presented in Fig. 3(e) to demonstrate variation of n_g in subsequent discharge pulses (about 12%–34%). Thus, substantial variation of T_{g0} and n_{g0} prior to each discharge pulse in the burst is expected, which causes relatively large variation of discharge parameters observed in the experiments as shown in Fig. 3. Note that substantially lower E_{pulse} for pulse Nos. 2–20 (2.6–3.8 mJ) compared to pulse No. 1 (5.2 mJ) indicate that the pulser was better matched with the load (discharge gap filled with plasma) on the first pulse (impedance immediately after the breakdown was ~1 kΩ as one can estimate from Fig. 2) rather than for subsequent pulses (impedance immediately after the breakdown was ~100–150 Ω according to Fig. 4). Correspondingly, this reduction in E_{pulse} for pulse No. 2–20 caused about fourfold reduction in the peak electron number density observed experimentally.

The evolution of discharge parameters for a burst of 20 pulses at a repetition rate of $f = 100$ kHz is presented in Fig. 5. n_e was determined from CMS measurements using same approximation for $V = 2.5\times10^{-4}$ cm^3, while ν_m approximation in the form of $\nu_m = \frac{1.42\times10^{12}}{2.5\times10^{19}} n_{g0}(\text{cm}^{-3})$, s^{-1} based on measured n_{g0} values was applied starting pulse No. 2 only (given that n_g experienced very minor variations of 5%–10% starting pulse No. 2). For pulse No. 1, the temporal evolution of ν_m was used for n_e determination based on temporally resolved measurements of n_g by laser Rayleigh scattering reported in Refs. 8 and 18.

Similar to the 10 kHz case, memory effects were obviously present causing variation of the discharge pulse parameters from that of the first pulse. Steady-state discharge pulse parameters at 100 kHz were reached at about pulse No. 5 and were associated with lower variability compared to the 10 kHz case ($V_{br} = 6$ kV, $I_{peak} = 23$ A, $E_{pulse} = 1.4$ mJ, $T_{g0} = 5000$ K, $n_{g0} = 0.25\times10^{19}$ cm^{-3}, and $n_{e,peak} = 1.5\times10^{15}$ cm^{-3} with corresponding variations of ±12%, ±5%, ±6%, ±2%, ±20%, and ±3%, respectively). Smaller variability in the steady-state is associated with short time (10 μs) between the pulses so that gas properties T_g and n_g did not change significantly on that inter-pulse timescale. This is supported by the n_g plot in Fig. 5(e) showing very minor variation between n_{g0} and $n_{g,min}$ (about 5%–10%) starting pulse No. 2. Even lower pulse energy $E_{pulse} = 1.4$ mJ in the steady-state of the 100 kHz NRP discharge compared to the 10 kHz counterpart (3.2 mJ) indicate even greater pulser's mismatch with the discharge gap load (impedance immediately after breakdown was ~75 Ω according to Fig. 6). This smaller steady-state pulse energy for the 100 kHz NRP discharge correspondingly led to smaller electron number density. Specifically, fourfold reduction in E_{pulse} for pulse Nos. 2–20 compared to the first pulse (from 5.2 to 1.2 mJ) observed for the 100 kHz NRP discharge caused corresponding tenfold reduction in the peak electron number density (from 1.5×10^{16} to 1.5×10^{15} cm^{-3}).

Figure 5(f) allows the direct comparison of the electron decay of single-pulse ns-discharge (based on pulse No. 1) and steady-state

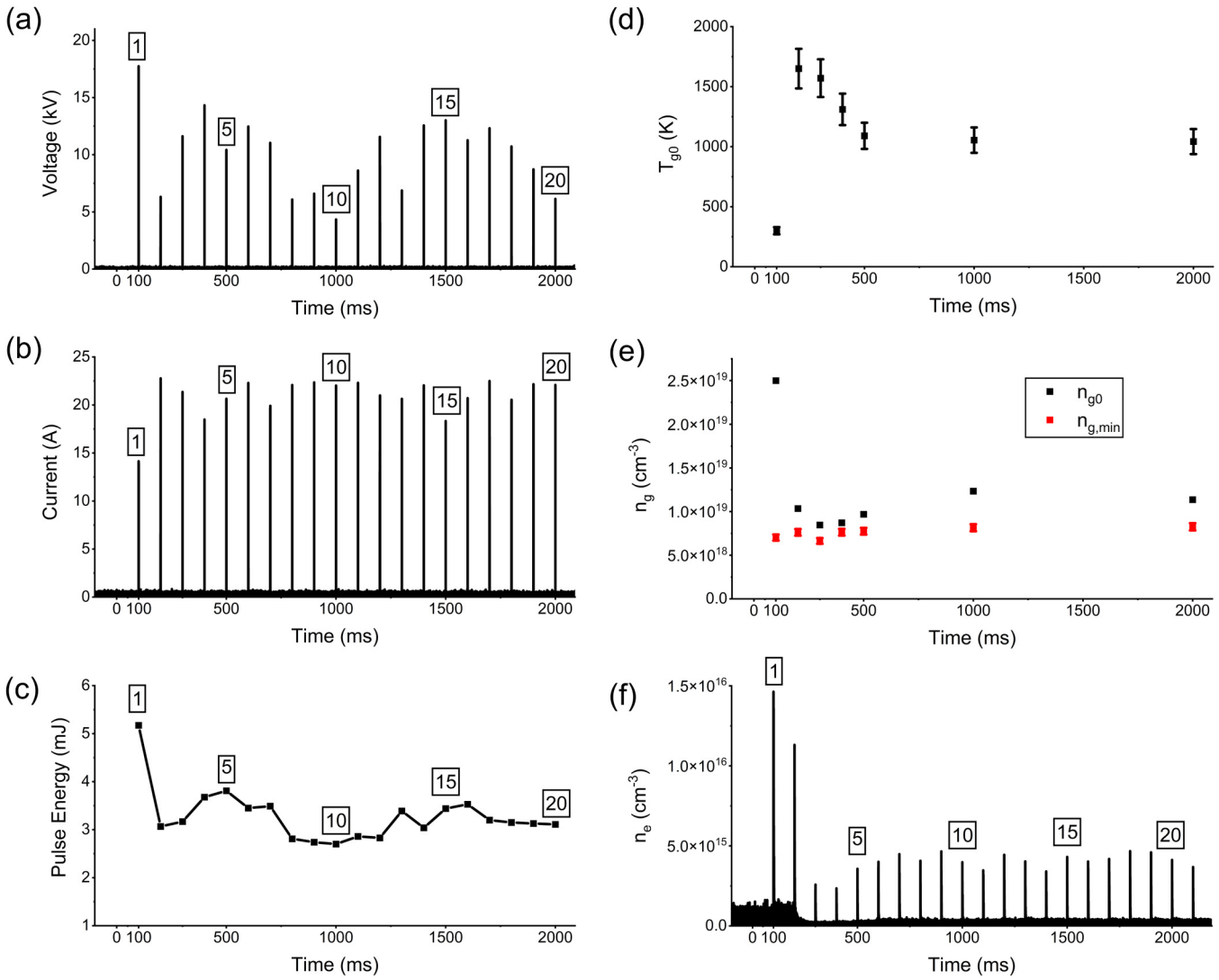

FIG. 3. Temporal evolution of parameters for NRP discharge at f = 10 kHz. (a) Voltage (V_d); (b) current (I_d); (c) discharge pulse energy (E_{pulse}); (d) gas temperature T_{g0} right before discharge pulse initiation for pulse Nos. 1, 2, 3, 4, 5, 10, and 20; (e) gas number density n_{g0} right before discharge pulse initiation (black) and minimum gas density $n_{g,min}$ after each discharge (red) for pulse Nos. 1, 2, 3, 4, 5, 10, and 20; and (f) electron number density n_e.

of the 100 kHz NRP discharge (after pulse No. 5). For the single-pulse ns-discharge, the characteristic decay time was 150–200 ns (corresponding decay rate of 0.5–0.7 × 10^7 s^{-1}), while for the steady-state of the 100 kHz NRP discharge, it increased to 400–700 ns (decay rate of 0.14–0.25 × 10^7 s^{-1}). In general, the electron decay is driven by dissociative recombination ($X_2^+ + e \rightarrow X + X$, where X is N or O) and three-body attachment to oxygen ($e + O_2 + X_2 \rightarrow O_2^- + X_2$, where X is N or O) governed by the following equation: $\frac{dn_e}{dt} = -\beta n_e^2 - \nu n_e$.[8] We have numerically simulated this equation using electron temperatures in the range of 0.3–3 eV, dissociative recombination rate for oxygen and nitrogen $\beta = 2 \times 10^{-7} \times \sqrt{\frac{300}{T_e}}$ (cm^3 s^{-1}), and three-body attachment rate to oxygen $\nu = k_1 n_{O_2}^2 + k_2 n_{O_2} n_{N_2}$, where $k_1 = 1.4 \times 10^{-29} \times \frac{300}{T_e} \times \exp\left(-\frac{600}{T_{gas}}\right) \times \exp\left(\frac{700 \times (T_e - T_{gas})}{T_e \times T_{gas}}\right)$ (cm^6 s^{-1}) and $k_2 = 1.07 \times 10^{-31} \times \left(\frac{300}{T_e}\right)^2 \times \exp\left(-\frac{70}{T_{gas}}\right) \times \exp\left(\frac{1500 \times (T_e - T_{gas})}{T_e \times T_{gas}}\right)$ (cm^6 s^{-1}).[21,22] Contribution of dissociative recombination was dominant in the initial portion of the electron decay for both single-pulse ns-discharge and 100 kHz NRP discharge. Numerical simulations yield substantially faster decay times (1–2 orders of magnitude) in comparison to the experimentally measured ones; namely, $T_e = 0.3$, 1 and 3 eV yield decay times of 1, 2, and 4 ns for the single-pulse discharge and 8, 15, and 26 ns for 100 kHz NRP

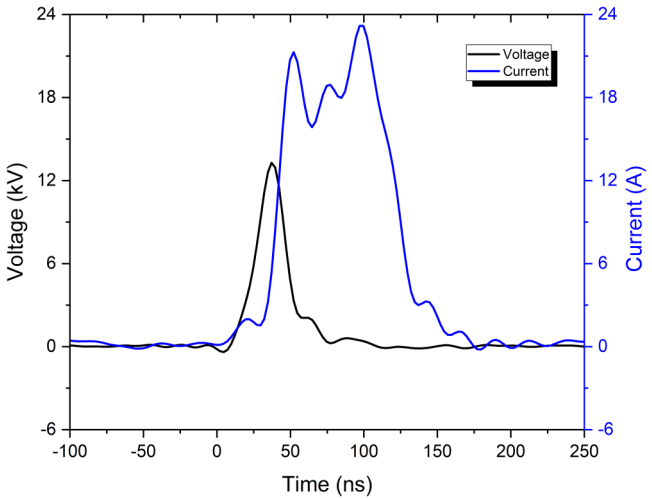

FIG. 4. Typical temporal evolution of discharge voltage (black) and discharge current (blue) for pulses in the burst (f = 10 kHz, pulse No. 10).

discharge in the steady-state. The observed discrepancy can be potentially attributed to inapplicability of rate coefficients available in literature to conditions of NRP discharges (due to high gas temperatures, the presence of excited ions rather than in the ground state)[8] and to additional ionization of gas after ns-pulse in collisions of electrons with excited gas particles.

For repetition frequencies of 1–100 kHz considered in this work, the memory effects can be attributed to the reduction in gas number density (increase in the reduced electric field E/n_g) and increase in the gas temperature as these parameters recover to initial unperturbed values of 2.5×10^{19} cm^{-3} and 300 K on the corresponding timescale of about 1 ms. Changes of n_{g0} and T_{g0} in the subsequent discharge pulses after pulse No. 1 along with variation of the pulser matching conditions cause corresponding changes in V_{br} (refers to the effect of dielectric strength recovery), I_{peak}, E_{pulse}, and $n_{e,peak}$. An additional mechanism that operates on the similar timescale and can potentially contribute to the observed memory effects is residual positive space charge remaining in the discharge gap.[23] Electron number density decays on faster timescale of several μs, so that these residual electrons should be expected to contribute to the memory effects at higher discharge repetition frequencies (>100 kHz).

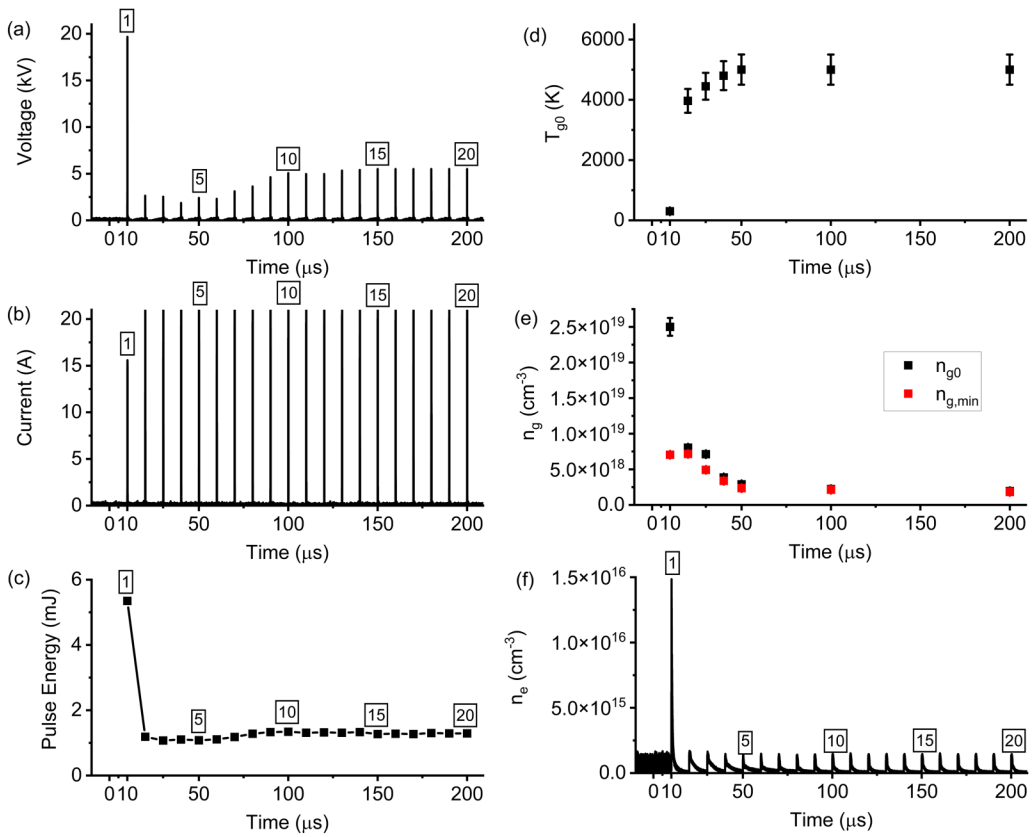

FIG. 5. Temporal evolution of parameters for NRP discharge at f = 100 kHz. (a) Voltage (V_d); (b) current (I_d); (c) discharge pulse energy (E_{pulse}); (d) gas temperature T_{g0} right before discharge pulse initiation for pulse Nos. 1, 2, 3, 4, 5, 10, and 20; (e) gas number density n_{g0} right before discharge pulse initiation (black) and minimum gas density $n_{g,min}$ after each discharge (red) for pulse Nos. 1, 2, 3, 4, 5, 10, and 20; and (f) electron number density n_e.

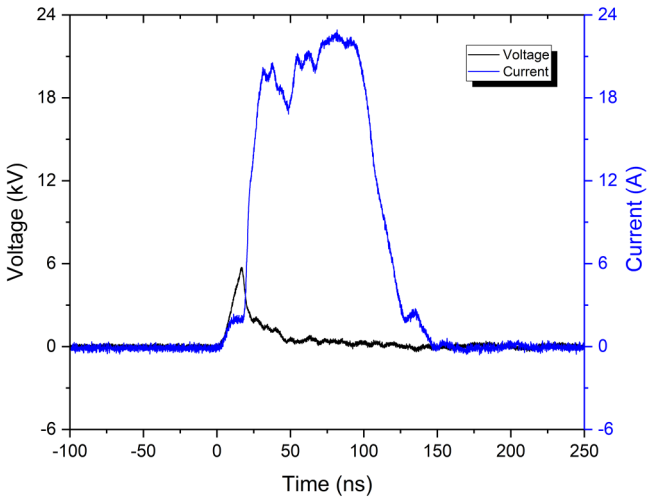

FIG. 6. Typical temporal evolution of discharge voltage (black) and discharge current (blue) for pulses in the burst (f = 100 kHz, pulse No. 10).

IV. CONCLUSIONS

Initial transient stage of NRP pin-to-pin discharges is associated with first several discharge pulses, e.g., first five (5) pulses for the case of few mJ nanosecond discharge pulses, 5 mm discharge gap, and 100 kHz repetition frequency used in this work. Conditions of the gas in the discharge gap significantly change during these initial pulses leading to manifold reduction in gas number density and increase in gas temperature. This, in turn, affects impedance of the interelectrode gap filled with plasma during the discharge and, correspondingly, changes energy deposition into the gap in subsequent discharge pulses. In general, electron decay after individual discharge pulses is governed by contributions of dissociative recombination and electron attachment to oxygen, while dissociative recombination is expected to dominate the initial portion of the decay. Relatively slow measured electron decay can be potentially attributed to inapplicability of reaction rate coefficients available in literature to conditions of NRP discharges and to additional ionization of gas after ns discharge pulses in collisions of electrons with excited gas particles.

ACKNOWLEDGMENTS

The authors would like to thank N. A. Popov, M. N. Shneider, and S. Bane for valuable discussions. This work was supported by the U.S. Department of Energy (Grant No. DE-SC0018156) and partially by the National Science Foundation (NSF) (Grant No. 1903415).

AUTHOR DECLARATIONS

Conflict of Interest

The authors have no conflicts to disclose.

Author Contributions

Xingxing Wang: Data curation (lead); Methodology (lead); Visualization (lead); Writing – original draft (equal); Writing – review and editing (equal). **Adam Patel:** Data curation (supporting); Methodology (supporting); Writing – original draft (supporting). **Alexey Shashurin:** Conceptualization (lead); Data curation (supporting); Funding acquisition (lead); Methodology (supporting); Project administration (lead); Resources (lead); Supervision (lead); Validation (lead); Writing – original draft (equal); Writing – review and editing (equal).

DATA AVAILABILITY

The data that support the findings in this study are available from the corresponding author upon reasonable request.

REFERENCES

[1]S. M. Starikovskaia, N. B. Anikin, S. V. Pancheshnyi, D. V. Zatzepin, and A. Y. Starikovskii, Plasma Sources Sci. Technol. **10**, 344 (2001).
[2]W. Kim, M. Godfrey Mungal, and M. A. Cappelli, Combust. Flame **157**, 374 (2010).
[3]Q. L. L. Pham, D. A. Lacoste, and C. O. Laux, IEEE Trans. Plasma Sci. **39**, 2264 (2011).
[4]G. L. Pilla, D. A. Lacoste, D. Veynante, and C. O. Laux, IEEE Trans. Plasma Sci. **36**, 940 (2008).
[5]D. V. Roupassov, A. A. Nikipelov, M. M. Nudnova, and A. Y. Starikovskii, in *46th AIAA Aerospace Sciences Meeting and Exhibit* (AIAA, 2008), p. 47.
[6]J. Little, K. Takashima, M. Nishihara, I. V. Adamovich, and M. Samimy, AIAA J. **50**, 350 (2012).
[7]S. Samukawa, M. Hori, S. Rauf, K. Tachibana, P. J. Bruggeman, G. Kroesen, J. C. Whitehead, A. B. Murphy, A. F. Gutsol, S. Starikovskaia, U. Kortshagen, J. P. Boeuf, T. J. Sommerer, M. J. Kushner, U. Czarnetzki, and N. Mason, J. Phys. D: Appl. Phys. **45**, 253001 (2012).
[8]X. Wang, A. Patel, S. Bane, and A. Shashurin, J. Appl. Phys. **130**, 103303 (2021).
[9]N. A. Popov, Plasma Sources Sci. Technol. **25**, 044003 (2016).
[10]B.-D. Huang, K. Takashima, X.-M. Zhu, and Y.-K. Pu, J. Phys. D: Appl. Phys. **47**, 422003 (2014).
[11]P. S. Hsu, S. Roy, Z. Zhang, J. Sawyer, M. N. Slipchenko, J. G. Mance, and J. R. Gord, Opt. Lett. **41**, 1570 (2016).
[12]J. Miles, C. Murray, A. Ross, K. Lemmer, J. Russell, and S. Adams, Plasma Sources Sci. Technol. **29**, 07LT02 (2020).
[13]D. Z. Pai, D. A. Lacoste, and C. O. Laux, J. Appl. Phys. **107**, 093303 (2010).
[14]D. Z. Pai, D. A. Lacoste, and C. O. Laux, Plasma Sources Sci. Technol. **19**, 065015 (2010).
[15]D. L. Rusterholtz, D. A. Lacoste, G. D. Stancu, D. Z. Pai, and C. O. Laux, J. Phys. D: Appl. Phys. **46**, 464010 (2013).
[16]R. M. van der Horst, T. Verreycken, E. M. van Veldhuizen, and P. J. Bruggeman, J. Phys. D: Appl. Phys. **45**, 345201 (2012).
[17]X. Wang and A. Shashurin, AIAA J. **58**, 3245 (2020).
[18]X. Wang, A. R. Patel, and A. Shashurin, J. Appl. Phys. **129**, 183302 (2021).
[19]A. R. Patel, A. Ranjan, X. Wang, M. N. Slipchenko, M. N. Shneider, and A. Shashurin, Sci. Rep. **11**, 23389 (2021).
[20]B. Singh, L. K. Rajendran, J. Zhang, P. P. Vlachos, and S. P. M. Bane, Phys. Rev. Fluids **5**, 114501 (2020).
[21]A. Dogariu, M. N. Shneider, and R. B. Miles, Appl. Phys. Lett. **103**, 224102 (2013).
[22]I. A. Kossyi, A. Y. Kostinsky, A. A. Matveyev, and V. P. Silakov, Plasma Sources Sci. Technol. **1**, 207 (1992).
[23]X. Wang and A. Shashurin, Plasma Sources Sci. Technol. **26**, 02LT02 (2017).